Rapid prototyping of cost efficient X-ray collimators

J.C. Khong[1], R. Speller[1], S. Dorkings[2], K. Moss[2] and R. Moss[1]

[1]*Department of Medical Physics and Biomedical Engineering, University College London, Gower Street, London, WC1E 6BT, UK*

[2]*Defence Science and Technology Laboratory Fort Halstead, Sevenoaks, Kent, TN14 7BP, UK*

* Corresponding author: J.C. Khong
E-mail address: j.c.khong@ucl.ac.uk

Abstract

This paper reports on a novel technique for rapid and cost effective manufacture of bespoke X-ray shielding. This technique is particularly well suited for producing prototypes of complex collimators for proof of concept and/or short duration usage. Instead of heavily investing in state-of-the-art 3D metal printing to create X-ray collimators, a conventional plastic 3D printer was used to create a hollow shell of the correct geometry which was filled with tungsten powder as the X-ray attenuating material. In this paper we have applied this technique to produce a complex collimator for energy dispersive X-ray diffraction (EDXRD), which could not be manufactured using conventional machining methods. We compare the performance of this collimator to a solid tungsten 3D printed example of the same design. EDXRD shows that the two collimators have very similar performance with the backfilled collimator having marginally worse peak resolution in momentum transfer, which is attributed to X-ray transmission through the plastic walls and the much lower packing fraction of the tungsten powder. This technique is widely accessible and is capable of rapid prototyping complicated collimator designs, whilst at 1% the cost of using a

tungsten 3D printing technique.

Introduction

X-ray diffraction (XRD) is a widely used technique in chemistry, material science, engineering and biological research to provide non-destructive material identification and characterisation. Two different techniques; energy dispersive X-ray diffraction (EDXRD) and angular dispersive X-ray diffraction (ADXRD) are used to resolve the Bragg's equation (Eq. 1) in order to obtain the material crystal structure.

$$n\lambda = 2\text{d}\sin\theta \qquad (1)$$

Each has their own advantages. EDXRD uses white beam X-rays (containing a range of X-ray energies or wavelength, λ) with an energy sensitive detector to acquire diffracted X-ray signals as a function of X-ray energy at a defined angle (2θ). This is achieved using a specially designed collimator [1, 2]. In contrast, ADXRD uses monochromatic X-rays (fixed λ) and measures the diffracted X-ray signal over a range of angles.

EDXRD can be achieved with a small X-ray tube and an energy resolving X-ray detector to produce a compact X-ray diffraction system [3-5]. It could be incorporated into field deployable systems with portable material identification capabilities, which can be useful for applications such as defence and security, and in field archaeological analysis. Recently, we demonstrated the advantages of combining ADXRD and EDXRD to acquire the diffraction information with a pixelated, energy resolving sensor (HEXITEC) developed by RAL [5, 6]. The combination of techniques enables the system to collect more diffraction data and provide accurate analysis in a short timeframe. To ensure XRD measurements can be made from thick objects, a unique X-ray collimator positioned in front of the detector is used to select a specific scattering volume at a given depth or location

within the sample.

There have been several examples of collimators used for EDXRD systems including simple geometry such as slits [1, 7-9], pin-holes [10, 11], conical collimators [12, 13], and more complex arrangements [14-17], each having their own advantages and disadvantages. Factors such as diffraction angle, momentum transfer (Q) range, scattering volume, X-ray energy, spectra resolution, channel spacing, collimator length, and system size have to be considered while designing a collimator. For example, Schlesinger and Bomsdorf [16] model two types of collimators for pencil-beam and fan-beam setups that are capable of spatially resolved EDXRD measurements. The pencil-beam collimator consisted of separate ring-shaped segments and a Soller-slit type collimator to achieve fan-beam collimation. It was stated that such collimators are technically challenging to manufacture and they proposed using an additive manufacturing method, however, this would be very costly to produce.

In this paper, we report a technique for rapid prototyping EDXRD collimator with conventional 3D polylactic acid (PLA) printer from CAD models that can be tested using Geant4 Monte Carlo simulation. The effectiveness of the newly manufactured collimator has been demonstrated against a caffeine test sample illuminated by 100keV X-rays.

Methods

Manufacture of the collimator

The EDXRD collimator was designed using Solidworks CAD software (Solidworks 2016 x64 Edition) and the EDXRD effects were simulated using Geant4 Monte Carlo software (Geant4 10.2 patch-01) and CADMesh (Version 1.0). The collimator model (Fig. 1a) has been modified to be a hollow shell (Fig. 1b) using Solidworks with a wall thickness of 0.43 mm, except the top and base which were set to 2 mm. The top 2 mm section was printed as a separate part in order to use it as a lid to seal the collimator. A 15 mm diameter beam stop to absorb the X-rays directly penetrating through the sample is also included in the design.

The models were 3D printed using the 0.4mm nozzle and PLA material (Ultimaker PLA ⌀2.85mm) with a conventional Ultimaker Extended 2+ 3D printer. A 4mm borosilicate build plate was used, with a 1mm thick copper plate sandwiched between it and the heat plate to create a more homogenous build plate temperature. The layer height, print speed and build plate temperature were set to be 0.06 mm, 40 mm/s and 73 °C respectively, with other settings at default. A 10 mm height raft was added into the model as a sacrificial material during 3D printing to prevent deformation of the collimator channels due to a combination of the weight of the printed part and the softening effect of being in close contact to the heated bed. This enabled high precision channels to be formed (Fig. 1b). The hollow collimators (Fig. 1c) were then filled with 1-5 μm tungsten (W) powders (Alfa Aesar, CAS no. 7440-33-7). A laboratory dental shaker was used during the filling process to ensure the collimator shell was as densely packed as possible. The lid was then sealed using adhesive (Fig. 1c) to contain all the powder. Using the CAD model volumes for the hollow collimator and tungsten filled collimator, the tungsten packing density could be

determined. The filled collimator had a tungsten powder packing fraction of 34.2%, while the tungsten 3D printed collimator (Fig.1c far right) had an effective packing fraction of 88.0% to 93.3%, in agreement with the manufacturer's specifications.
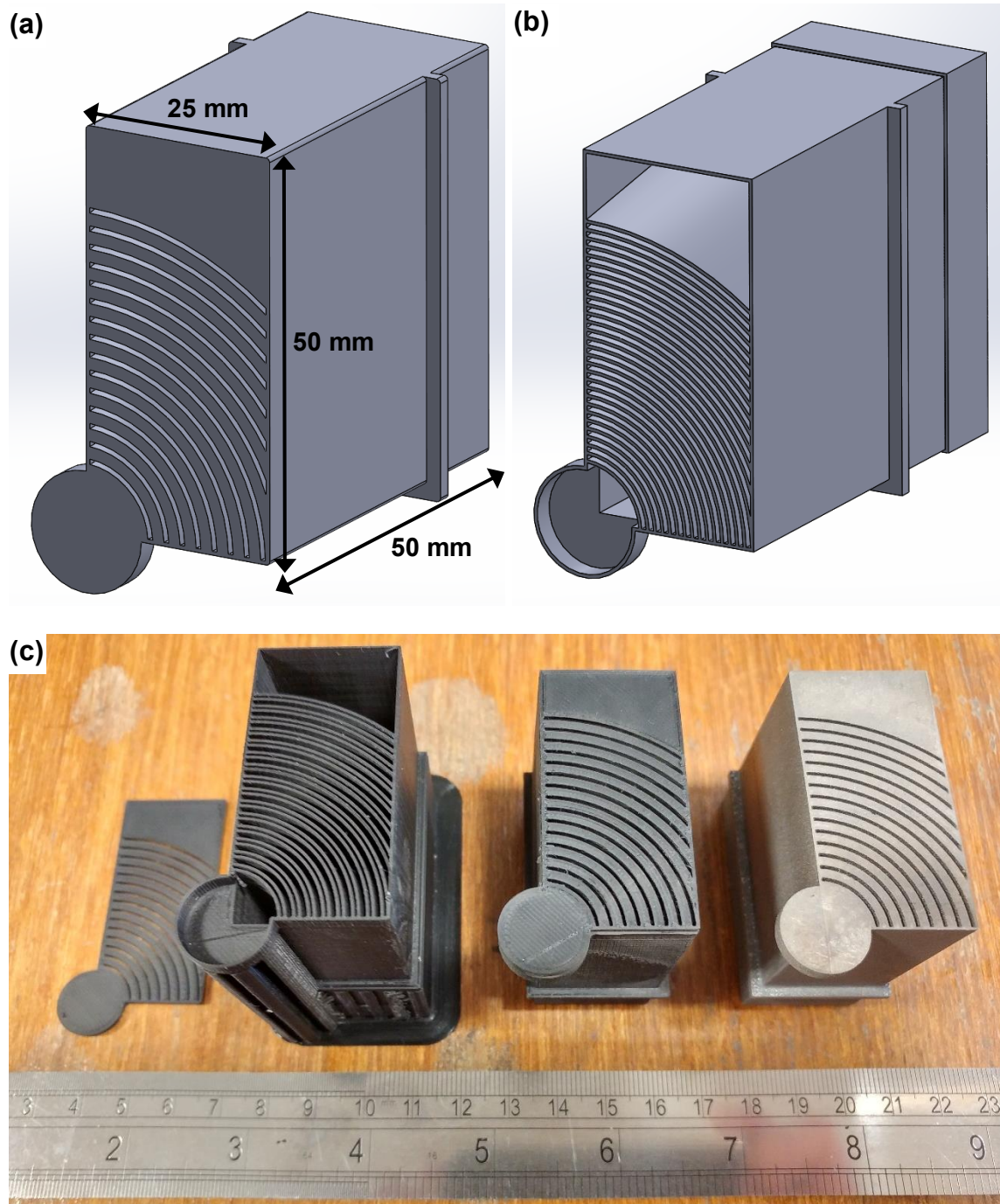

Figure 1: EDXRD collimator designed by UCL. (a) CAD model of the optimised collimator (b) CAD model of the collimator outer shell (c) from the left an example of a 3D printed PLA collimator shell (this is with different channel widths), W-filled collimator and W-printed collimator.

Experimental setup and data collection

Caffeine powder (Sigma-Aldrich, CAS No. 58-08-2) was used as a standard to investigate the performance of the 3D printed tungsten filled collimator. A thin walled (0.43 mm) container was 3D printed to hold a 10 mm thick caffeine powder sample (Fig. 2b) and was used to characterise the response of both collimator arrangements.

Fig. 2a and Fig. 2b show the schematic diagram and the experimental setup of the EDXRD X-ray system. A standard X-ray tube (Thales THX 160 1055 tube with Gulmay generator and controller) was used at a constant accelerating potential of 100 kV. The tube power and focal spot were set to 1 kW and 5.5 mm (diameter) respectively. The X-ray beam was collimated with two 5 mm thick lead plates each with an opening of 0.5 mm diameter to define the primary beam. The lead plates were separated by 40 mm and the assembly was placed 50 mm from the X-ray tube focal spot. The sample was placed at a distance of 350 mm from the X-ray tube. The diffraction collimators were designed such that the distance between the scattering volume and the back side (the side facing the detector) of the collimator was 300mm. The caffeine sample was positioned 300 mm from the back surface of the collimator to place it within the scattering volume. This 3D printed tungsten filled collimator was placed in a rotary support system that could accommodate up to 6 collimators. This collimator support system was designed to ensure each collimator aligns with the X-ray beam and enabled rapid changing of collimators with repeatable accuracy. An 80 x 80 pixel (250 µm pitch) energy resolving detector (HEXITEC, STFC) was placed 5mm behind the collimator.

An instrument-specific data acquisition program was used to collect data with the

HEXITEC detector. The detector was calibrated using an ^{241}Am source (370 kBq). The output energy spectrum was set to cover the range 0-100keV with an energy bin width of 0.25 keV and a low energy threshold of 4 keV. For each data collection, diffraction patterns were collected with 600 seconds of exposure time to improve signal-to-noise ratio. In order to record the X-ray flux through the whole collimator it was necessary to move the detector between two positions. The detector was mounted on a small linear translation stage to accommodate the 20 mm shift between these positions. The measurements taken at each position were merged into a single image for further analysis.
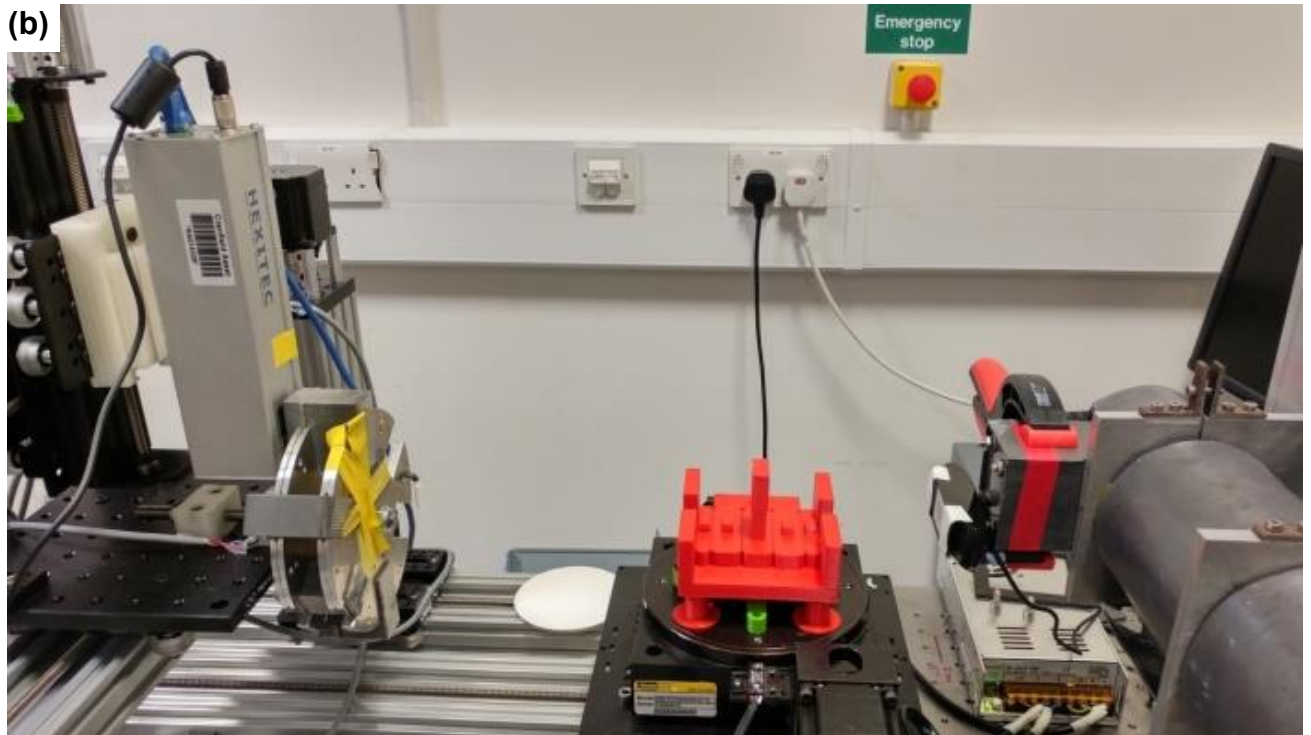
(a)

(b)
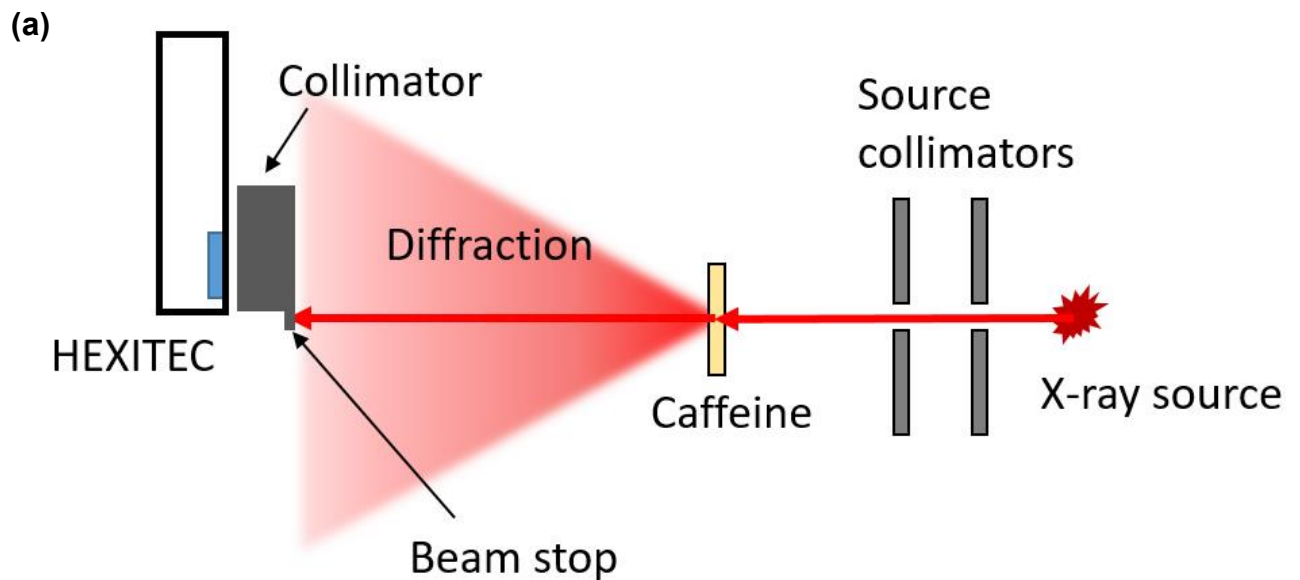
Figure 2: (a) A schematic diagram and (b) a snapshot of the experiment setup

Data analysis

The raw frame data from the detector were corrected for charge sharing by discrimination [18] and histogram plotted in energy. The data was imported into Matlab software as an 80 x 160 x 400 matrix (Fig. 3a) for further analysis using a script written for this specific collimator. The dead detector pixels were masked in Matlab with a zero value (appear as a black pixels in Fig. 3a). The detector captured counts in 15 angular channels which appear as bright arcs in Fig. 3a. Each channel angle was determined by taking a diffraction measurement of a 10 mm Aspirin sample (Cayman Chemical CAS No. 50-78-2), with the positions of the resulting diffraction peaks visible through each ring used to determine that ring's angle. The energy spectrum for pixels falling in each angular channel were summed together to produce 15 diffraction spectra. Since the scattering angle of each channel was known, the energy spectra from each channel converted to momentum transfer (Q)

via Eq. 2 where the product *hc* = 1.24 nm keV.

$$Q = \frac{E}{hc}\sin\theta \qquad (2)$$

The 15 1D spectra were then summed in *Q* to improve the statistical quality of the diffraction profile (Fig. 3b). The diffraction spectra obtained from the different collimators against the caffeine sample are plotted together with the caffeine standard (dotted line) from Crystallography Open Database (COD no. 2100202) [19] for comparison.
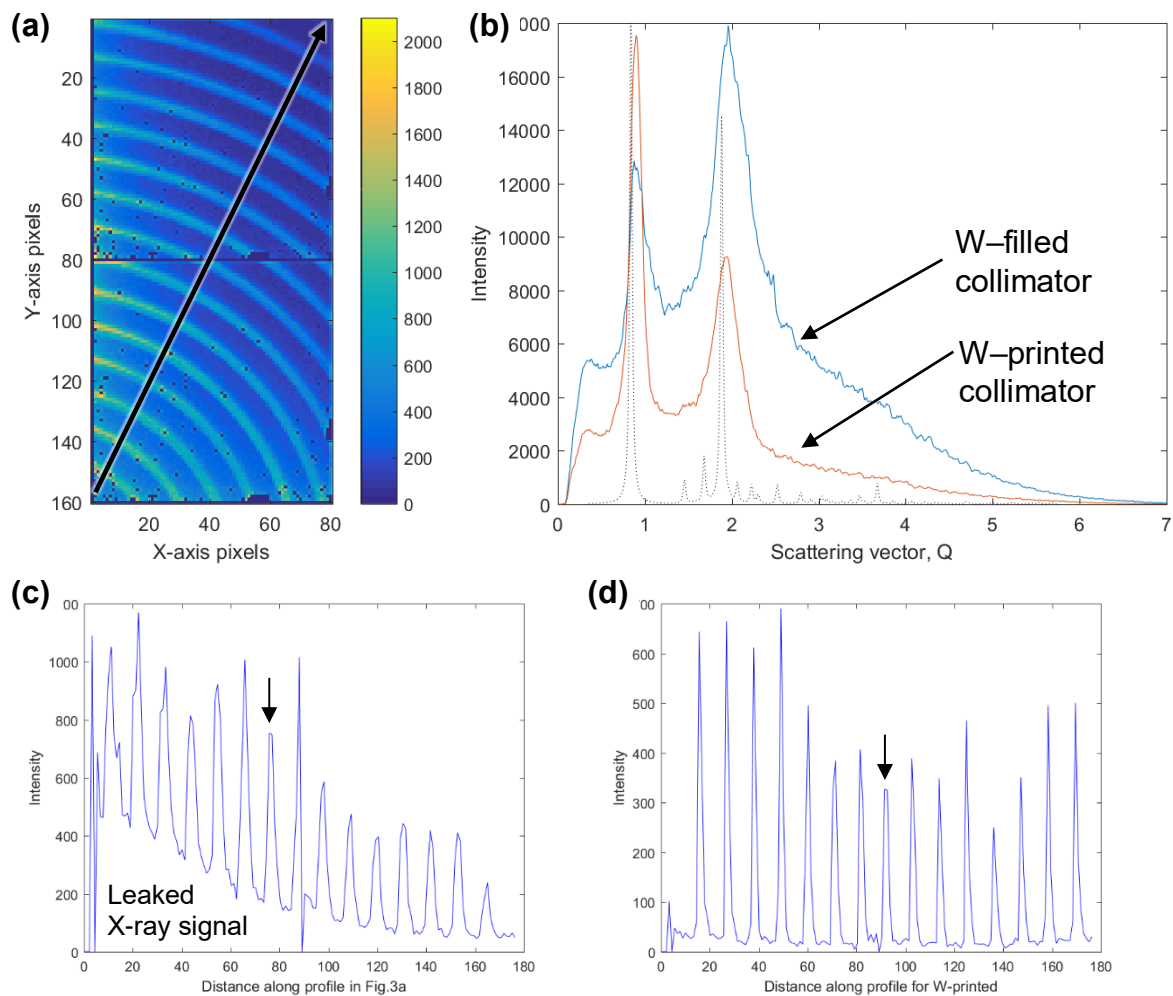

Figure 3: (a) Data collected by HEXITEC detector of caffeine diffraction pattern obtained using the W-filled collimator.; (b) sum of momentum transfer spectra of the 15 channels for the W-filled and W-printed collimators; transmission profile of the black diagnonal line inserted in Fig. 3a for (c) W-filled and (d) W-printed collimators.

Results and Discussion

The unique design of the 15 channel collimator allows the combination of AD and ED XRD using the pixellated energy sensitive detector making full use of the HEXITEC capabilities. This allows shorter data acquisition times which is desirable for a portable system. In addition the different angle channels provide energy sensitivity which is useful when allowing for different material attenuation.

Fig. 3a shows the summed intensity of all X-ray energies observed by the Hexitec detector behind the W-filled collimator with a caffeine diffraction sample positioned within its scattering volume. Fig. 3c and Fig.3d show the intensity profile taken along the line of the black arrow in Fig. 3a for the W-filled and W-printed collimator respectively. Both graphs show 15 peaks which correspond to the X-ray signal passing through the 15 channels of the collimator. Due to the lower attenuation of the PLA wall, the W-filled collimator has broader peaks in comparison to W-printed collimator. Peaks were selected from Fig. 3c and Fig. 3d (labeled with black arrow) for comparison. The full width half maximum (FWHM) were measured to be 2.5460 ± 0.1499 and 1.6761 ± 0.1351 pixel, respectively. The 2 peaks were selected from the respective profiles due to their positions at the middle of the collimator and have reasonable Gaussian peaks to fit to. It is possible to reduce the broadening effect by printing the shell with thinner walls (using a smaller nozzle), however this will greatly increase the printing time, for example with 0.25mm nozzle, the printing time will increase to nearly two days. It was decided that the increased printing time was not worth the greater resolution in our printed hollow collimators, which were only being used as prototypes prior to printing collimators from solid W.

Fig. 3b shows the summed caffeine XRD spectra converted into momentum transfer measured by the 15 channels from the W-filled and W-printed collimators. The result shows that both collimators are able to resolve features in the caffine diffraction profile. There is a ~16% increase in the FWHM of the diffraction peaks observed through the W-filled collimator compared to the W-printed collimator. For the 1st caffeine peak the increase is from 0.1514 ± 0.0012 to 0.1745 ± 0.0116 Å^{-1}, whereas for the 2nd caffeine peak the values are 0.3314 ± 0.010 to 0.3847 ± 0.0084 Å^{-1}. The additional background signal observed through the W-filled collimator might be a contributing factor to this increase in diffraction peak width. Fig. 3c shows the extent of the X-ray leakage through the W-filled collimator from the greatly increased background signal observed between the collimator channels. The background ideally should be near zero, however, the tungsten packing density of only only 34.2% for the W-filled collimator leads to some X-ray leakage. This could be improved by investigating different mixing and tamping techniques, different size ratios of tungsten powders to improve the packing density, or by increasing the collimator length to provide greater X-ray attenuation.

Despite these issues, the W-filled collimator still provides an excellent alternative to tranditional manufacturing methods or the significantly more expensive 3D W-printed option. The filled collimator cannot entirely replace those manufactured using existing methods due to the lower durablility of the printed shell and the lower packing ratio of the tungsten, but it is a suitable technique to use for prototype collimators or for short duration applications. The capability for in house manufacturing of complicated collimator designs will greatly improve the development of EDXRD X-ray systems and complex X-ray shielding in general. In

addition, the comsumable cost to manufacture such collimators is £25 (approximately £2 for 3D printer filament and £23 for tungsten powder) in comparison to the 3D tungsten printed version at £2500.

Conclusions

PLA 3D printed hollow collimators, backfilled with tungsten powder have been compared to complex and expensive solid tungsten alternatives. X-ray diffraction measurements show that the W-filled collimator is an excellent substitute for a solid metal version with only 16% increase in FWHM of XRD spectra observed through the collimator. This technique allows rapid prototyping of complicated collimators at a fraction of the cost of other techniques.

Acknowledgement

Author contributions

J.C. Khong led the design of the concept, design and manufacturing of the collimator, X-ray experiments and analysed the X-ray diffraction data with the advice from R. Moss and R. Speller. J. C. Khong, R. Moss and R. Speller led the writing of the papers. All authors contributed to reviewing the manuscript.

Competing financial interests: The authors declare no competing financial interests.

Reference

[1] Bordas, J. and J. Randall, *Small-angle scattering and diffraction experiments in biology and physics employing synchrotron radiation and energy-dispersive techniques.* Journal of Applied Crystallography, 1978. **11**(5): p. 434-441.

[2] Kämpfe, B., F. Luczak, and B. Michel, *Energy Dispersive X‑Ray Diffraction.* Particle & Particle Systems Characterization, 2005. **22**(6): p. 391-396.

[3] Peterzol, A., et al., *Modeling-based optimization study for an EDXRD system in a portable configuration.* Nuclear Instruments and Methods in Physics Research Section A: Accelerators, Spectrometers, Detectors and Associated Equipment, 2011. **654**(1): p. 450-463.

[4] Moss, R., et al., *miniPixD: a compact sample analysis system which combines X-ray imaging and diffraction.* Journal of Instrumentation, 2017. **12**(02): p. P02001.

[5] O'Flynn, D., et al., *Identification of simulants for explosives using pixellated X-ray diffraction.* Crime Science, 2013. **2**(1): p. 4.

[6] Seller, P., et al., *Pixellated Cd (Zn) Te high-energy X-ray instrument.* Journal of Instrumentation, 2011. **6**(12): p. C12009.

[7] Baublitz Jr, M.A., V. Arnold, and A.L. Ruoff, *Energy dispersive x‑ray diffraction from high pressure polycrystalline specimens using synchrotron radiation.* Review of Scientific Instruments, 1981. **52**(11): p. 1616-1624.

[8] YangDai, T. and L. Zhang. *Collimators optimization for EDXRD security screening system*. in *Selected Papers of the Chinese Society for Optical Engineering Conferences held October and November 2016*. 2017. International Society for Optics and Photonics.

[9] Pandey, K., et al., *Energy-dispersive X-ray diffraction beamline at Indus-2 synchrotron source.* Pramana, 2013. **80**(4): p. 607-619.

[10] Brister, K.E., Y.K. Vohra, and A.L. Ruoff, *Microcollimated energy-dispersive x-ray diffraction apparatus for studies at megabar pressures with a synchrotron source.* Review of scientific instruments, 1986. **57**(10): p. 2560-2563.

[11] Egan, C.K., et al., *Full-field energy-dispersive powder diffraction imaging using laboratory X-rays.* Journal of Applied Crystallography, 2015. **48**(1): p. 269-272.

[12] Benedict, U. and C. Dufour, *Evaluation of high pressure x-ray diffraction data from energydispersive conical slit equipment.* High Temp. High Pressures, 1984. **16**: p. 501-504.

[13] Li, F., Z. Liu, and T. Sun, *Energy-dispersive small-angle X-ray scattering with cone collimation using X-ray capillary optics.* Review of Scientific Instruments, 2016. **87**(9): p. 093106.

[14] Bergmann, A., et al., *Improvement of SAXS measurements on Kratky slit systems by Göbel mirrors and imaging-plate detectors.* Journal of applied crystallography, 2000. **33**(3): p. 869-875.

[15] Korsunsky, A.M., et al., *Polycrystal deformation analysis by high energy synchrotron X-ray diffraction on the I12 JEEP beamline at Diamond Light Source.* Materials Letters, 2010. **64**(15): p. 1724-1727.

[16] Schlesinger, S. and H. Bomsdorf. *Simulation based collimator design for X-ray diffraction imaging using the GATE toolkit*. in *Imaging Systems and Techniques (IST), 2014 IEEE International Conference on*. 2014. IEEE.

[17] Mostafavi, M., et al., *Dynamic contact strain measurement by time‑resolved stroboscopic energy dispersive synchrotron X‑ray diffraction.* Strain, 2017. **53**(2).

[18] Veale, M., et al., *Measurements of charge sharing in small pixel CdTe detectors.* Nuclear Instruments and Methods in Physics Research Section A: Accelerators, Spectrometers, Detectors and Associated Equipment, 2014. **767**: p. 218-226.

[19] Derollez, P., et al., *Ab initio structure determination of the high-temperature phase of anhydrous caffeine by X-ray powder diffraction.* Acta Crystallographica Section B: Structural Science, 2005. **61**(3): p. 329-334.